*In press in Marine Ecology Progress Series (*doi: 10.3354/meps11558)

Nutrient supply controls picoplankton community structure during three contrasting seasons in the northwestern Mediterranean Sea

Running page head: Control of nutrient supply on picoplankton groups

Key words: turbulence, nutrient supply, Margalef´s mandala, picoplankton, Mediterranean Sea

Beatriz Mouriño-Carballido[1*], Elena Hojas[1], Pedro Cermeño[2], Paloma Chouciño[1], Bieito Fernández-Castro[1], Mikel Latasa[3], Emilio Marañón[1], Xosé Anxelu G. Morán[3,4], Montserrat Vidal[5]

1. Departamento de Ecoloxía e Bioloxía Animal, Universidade de Vigo, 36310, Vigo (Ponteverdra), Spain
2. Instituto de Ciencias del Mar, Consejo Superior de Investigaciones Científicas, Passeig Maritim de la Barceloneta, 37-49, E-08003, Barcelona, Spain
3. King Abdullah University of Science and Technology (KAUST), Division of Biological and Environmental Sciences and Engineering, Red Sea Research Center, , Thuwal 23955-6900, Saudi Arabia
4. Centro Oceanográfico de Xixón, Instituto Español de Oceanografía, Avda. Príncipe de Asturias, 70 bis - 33212, Xixón, Spain
5. Departament d'Ecologia, Universitat de Barcelona, Av. Diagonal, 643, Edifici Margalef, 08028, Barcelona, Spain

* Corresponding author: bmourino@uvigo.es

Abstract

We investigated the influence of ocean mixing and nutrient supply dynamics on picoplankton community composition in the context of the Margalef´s mandala (1978). We analysed simultaneous measurements of microturbulence, nutrient concentration, and autotrophic and heterotrophic picoplankton properties, collected during three cruises carried out in the northwestern Mediterranean Sea in March (F1), April-May (F2) and September (F3) 2009. The three cruises sampled different oceanographic conditions, starting with early stages of the late winter-early spring bloom, followed by the late stage of the bloom, and finally summer stratification. As a result of the variability in vertical diffusivity and the nitrate gradient across the nitracline, nitrate vertical fluxes were higher during F1 (23±35 mmol m^{-2} d^{-1}), compared to F2 (0.4±0.2 mmol m^{-2} d^{-1}) and F3 (0.09±0.09 mmol m^{-2} d^{-1}). *Prochlorococcus* abundance was low when nitrate supply was high, *Synechococcus* exhibited highest abundances at intermediate levels of nitrate supply and highest irradiance during F2, whereas large and small picoeukaryotic groups increased their abundance under high nutrients supply in F1. No significant relationships between the abundance of high and low nucleic acid heterotrophic bacteria and nitrate supply were found. In agreement with Margalef's model, our results show different responses of picophytoplankton groups to nitrate supply, probably reflecting differences in nutrient uptake abilities, and that the ratio of prokaryotic to picoeukaryotic photoautotrophic biomass decreased with increasing nitrate supply.

1. Introduction

Picoplankton (ca. <2 μm in diameter) are the most abundant organisms in the ocean, often dominate planktonic biomass and primary production (Chisholm 1992, Marañón 2015), and they could represent a substantial contribution to carbon export (Richardson & Jackson 2007). The flow cytometric analysis of this planktonic size class allows the discrimination of two genera of picocyanobacteria (*Synechococcus* and *Prochlorococcus*), usually at least two groups of autotrophic picoeukaryotes (small and large), and two groups of heterotrophic bacteria according to their high nucleic acid (HNA) and low nucleic acid (LNA) content (Marie et al. 1999). Initially HNA bacteria were considered as the active fraction and LNA the dormant or dead cells. Although some studies have described similar growth rates for both groups (Longnecker et al. 2005, Scharek & Latasa 2007), HNA cells usually outgrow LNA cells worldwide (Gasol et al. 1999, Bouvier et al. 2007, Morán et al. 2011).

It could be tempting to treat picophytoplankton as a coherent ecological assemblage. However this view oversimplifies a large phylogenetic and metabolic diversity evidenced by their differential spatial distribution. *Prochlorococcus* is thought to be restricted to water temperatures above 15ºC, extending from the surface to about 150 m depth, in the open ocean between 40°N and 40°S (Chisholm et al. 1988, Partensky, Hess, et al. 1999, Johnson et al. 2006). The vertical distribution of *Synechococcus* is shallower than that of *Prochlorococcus*, but covers a wider geographical distribution, including both polar and high-nutrient waters (Partensky, Blanchot, et al. 1999, Li 2007, Flombaum et al. 2013). Picoeukaryotes are ubiquitous in surface waters and dominate the picoplankton community, together with *Synechococcus,* in coastal systems (Tarran et al. 2006, Schattenhofer et al. 2009, Sharples et al. 2009). These patterns suggest that

54 resource requirements may be important factors regulating the observed regional
55 distribution of picoplankton groups.
56 Nutrient supply into the surface ocean is driven by nutrient concentration but also by
57 mixing, as was first schematized by Margalef´s (1978), initially based upon his
58 observations in the Ría de Vigo (northwestern Spain). The original diagram (see Figure
59 2 in Margalef (1978)) predicts the occurrence of different phytoplankton functional
60 groups versus turbulent mixing (x-axis) and nutrient concentration (y-axis), based on
61 the selection of species-specific functional traits and survival strategies. According to
62 this conceptual model, high turbulence levels and massive and intermittent nutrient
63 supplies favour large-sized phytoplankton, primarily diatoms, which possess high
64 maximum uptake rates and the ability to store nutrients in large, intracellular vacuoles.
65 Conversely, motile species (dinoflagellates) and those with high affinity for nutrients
66 (coccolithophores), about half-way along, dominate in nutrient-impoverished stratified
67 systems. The diagonal between diatoms and dinoflagellates traces the trend in the
68 changing environment, and the main sequence from alternative fast-growing *r*-selected
69 to slower growing *K*-selected species (MacArthur & Wilson 1967, Pianka 1970). If
70 turbulence decays but free nutrients remain abundant, an alternative successional route
71 leads to the species forming harmful algal blooms. High turbulence and low nutrient
72 conditions are too harsh for phytoplankton life, and according to Margalef this domain
73 is empty, meaning that the life-forms found in such conditions are not adapted to them.
74 A reorientation of Margalef´s first plot was presented a year later to accommodate
75 alternative tracks in the main sequence that might result in red-tide formation (Margalef
76 et al. 1979). A recent review of Margalef´s model, including the discussion of its
77 dynamical features and its significance for blooms, has been provided by Wyatt (2014).

78 This model pioneered the use of trait-based approaches in phytoplankton ecology
79 (Litchman 2007). However, several studies carried out in the last decade noted a
80 number of limitations when applying this approach to the field. First, because the
81 Margalef´s mandala was conceived before the discovery of smaller-sized planktonic
82 groups (i.e. picoplankton <2 μm in diameter), it describes only the succession of
83 vegetative phases of microphytoplankton (Wyatt 2014). Moreover, due to the
84 methodological difficulties in quantifying mixing in the field, the validation of
85 Margalef´s model has been limited so far to studies where indirect estimates of nutrient
86 supply were used.
87 In 2009, we conducted simultaneous measurements of microstructure turbulence,
88 nutrient concentration and picoplankton abundance and cell properties in the
89 northwestern Mediterranean during three cruises. Although the Mediterranean Sea is
90 mostly an oligotrophic domain, the northwestern basin is characterized by moderate
91 levels of primary production (Estrada 1996, Morán & Estrada 2005). In winter, this
92 region is under the influence of strong wind bursts and intense cooling, which originate
93 a deep-mixed patch of dense water, sometimes extending from the surface down to
94 more than 2000 m (Leaman & Schott 1991). Convective mixing and the subsequent late
95 winter-early spring bloom after re-stratification are responsible for increasing primary
96 production in this region. Our three cruises sampled different oceanographic conditions,
97 starting with early stages of the late winter-early spring bloom, followed by the late
98 stage of the bloom, and ending with summer stratification. Here we analyze this data set
99 in order to investigate the response of picoplankton to different levels of mixing and
100 nutrient supply, as an attempt to integrate this fundamental group of planktonic
101 microorganisms within the Margalef's mandala conceptual framework.
102

2. **Methods**

Field data were collected during three cruises carried out on board BIO Sarmiento de Gamboa in the northwestern Mediterranean Sea in the framework of the FAMOSO (FAte of the northwestern Mediterranean Open sea Spring blOom) project. The three cruises, conducted in 2009, were designed to cover different stages starting with the late winter-early spring phytoplankton bloom in FAMOSO1 (F1, 14 -22th March), the post-bloom in FAMOSO2 (F2, 30th April -13th May) and the late stratification in FAMOSO3 (F3, 17-19th September). During these cruises, conductivity temperature depth (CTD) profiles were conducted with a SBE911plus probe (Sea-Bird Electronics) attached to a rosette equipped with Niskin bottles. Samples were collected on 19 CTD casts for the determination of dissolved inorganic nitrogen and phosphate, and picoplankton abundance and cell properties (see Table 1 and Figure 1). Wind speed data were collected by the on board meteorological station.

2.1. Determination of dissolved inorganic nitrogen and phosphate

Samples for dissolved inorganic nutrients analysis were collected at 7-9 depths in the upper 400 m, and filtered through precombusted (450°C, 4 h) 47 mm diameter Whatman GF/F filters in an acid-cleaned glass filtration system, under low N_2-flow pressure. Samples for dissolved inorganic nitrogen (nitrate plus nitrite) and phosphate determinations were collected in 30-ml polypropylene and 60-ml polycarbonate bottles, respectively, and those for nitrate plus nitrite kept frozen (−20°C) until analyses. Nitrate plus nitrite concentrations, thereafter nitrate, were measured spectrophotometrically with an Alliance Evolution II autoanalyzer following standard procedures (Grasshoff et al. 1999). The detection limit was 0.01 mmol N m^{-3}. Phosphate concentrations were determined immediately after collection manually using the procedure of Grasshoff et

al. (1999), with a Shimadzu UVprobe spectrophotometer using a 10 cm cuvette to increase the detection limit to 0.01 mmol P m^{-3}.

2.2. Flow cytometry

Samples for the determination of picoplankton abundance and cell properties were taken at 5-11 depths in the upper 200 m, with higher vertical resolution in the upper 80 m of the water column. Picoplankton samples (1.8 ml) were preserved with 1% paraformaldehyde + 0.05% glutaraldehyde (final concentration). Samples were frozen at −80 °C until analysis in the laboratory with a FACSCalibur flow cytometer (Becton-Dickinson) equipped with a laser emitting at 488 nm. For estimating the abundance of the different groups (cell ml^{-1}), calibration of the cytometer flow rate was performed daily. Two aliquots from the same sample were used for the study of picophytoplankton (0.6 ml) and heterotrophic bacteria (0.4 ml), analyzed at high (~/mean 52 µl min^{-1}) and low (~/mean 32 µl min^{-1}) flow rate, respectively. Before the analysis, the DNA of heterotrophic bacteria was dyed with fluorochrome 2.5 µmol l^{-1} SYTO-13.

Autotrophic cells were separated into two groups of cyanobacteria (*Synechococcus* and *Prochlorococcus*) and two groups of picoeukaryotes (large and small), based on their fluorescence and light scatter signals (SSC), as explained in Calvo-Díaz and Morán (2006). Two groups of heterotrophic bacteria were distinguished based on their relative green fluorescence (FL1, 530 nm), used as a proxy for nucleic acid content, referred to as high nucleic acid (HNA) and low nucleic acid (LNA) content bacteria.

In order to estimate biovolume, we used an empirical calibration between SSC and cell diameter (Calvo-Díaz & Morán 2006). Spherical shape was assumed for all the groups. Finally, picoplankton biomass was computed using the following conversion factors of volume to carbon: Norland (1993) for heterotrophic bacteria, 230 fg C $µm^{-3}$ for

153 *Synechococcus*, 240 fg C μm^{-3} for *Prochlorococcus* and 237 fg C μm^{-3} for
154 picoeukaryotes (Worden et al. 2004). More details about the processing and analysis of
155 flow cytometry samples are provided in Gomes et al. (2015).

156

157 *2.3. Measurements of dissipation rates of turbulent kinetic energy and estimates of*
158 *vertical diffusivity*

159 Measurements of dissipation rates of turbulent kinetic energy (ε) were conducted in 19
160 stations, down to a maximum depth of 340 m, by using a microstructure profiler (MSS,
161 ISW Wassermesstechnik, Prandke and Stips 1998) (see Table 1 and Figure 1). Sets of 6-
162 7 turbulence profiles were taken at each station. The profiler was equipped with two
163 velocity microstructure shear sensors (type PNS98), a microstructure temperature
164 sensor, a sensor to measure horizontal acceleration of the profiler, and high-precision
165 CTD sensors. Chlorophyll-*a* concentrations between 0.05 and 2.91 mg m^{-3},
166 fluorometrically determined from water samples collected in the upper 200 m, were
167 used to calibrate the CTD fluorometer (chlorophyll-*a* = 1.8906 x fluorescence – 0.2336
168 (R^2 = 0.71, n=83)). Details of chlorophyll-*a* determinations are given in Estrada et al.
169 (2014). The profiler was balanced to have negative buoyancy and a sinking velocity of
170 ~0.4-0.7 m s^{-1}. The frequency of data sampling was 1024 Hz. The calibration of the
171 shear sensors was performed just before the cruise and the sensitivity was checked daily
172 during the data processing. Due to significant turbulence generation close to the ship,
173 data shallower than 10 m were discarded. The squared Brunt-Väisälä frequency (N^2), a
174 proxy for water column stratification, was computed from the CTD profiles according
175 to the equation:

176 $$N^2 = -\left(\frac{g}{\rho_w}\right)\left(\frac{\partial \rho}{\partial z}\right) \quad (s^{-2}) \qquad (1)$$

where g is the acceleration due to gravity (9.8 m s^{-2}), ρ_w is seawater density (1025 kg m^{-3}), and $\frac{\partial \rho}{\partial z}$ is the vertical potential density gradient.

ε and N^2 were averaged over depth intervals of 10 m length. The data processing was carried out with the commercial MSSpro software, which included the removal of spiky data, as described in detail in Mouriño-Carballido et al. (2011).

Vertical diffusivity (Kz) was estimated as:

$$Kz = e\frac{\varepsilon}{N^2} \qquad (2)$$

Where e is the mixing efficiency, here considered as 0.2 (Osborn 1980), as supported by the comparison of microstructure measurements and tracer release experiments both in the open ocean and coastal waters (Ledwell et al. 2000, Oakey & Greenan 2004, Gregg et al. 2012).

Vertical diffusive fluxes of nitrate were calculated, following the Fick´s law, from the product of the nitrate gradient across the nitracline and the averaged Kz for the same depth interval (Sharples et al. 2001, Fernández-Castro et al. 2015). The nitrate gradient was obtained by linearly fitting nitrate concentrations in the nitracline, determined as the region of approximately maximum and constant gradient, usually including 3-6 nitrate data points.

2.4 Light availability

A Licor Photosynthetically Active Radiation (PAR) sensor placed on the CTD probe was used to obtain vertical profiles of PAR irradiance throughout the water column. The vertical attenuation coefficient was calculated using the Beer-Lambert Law equation (Kirk 1994). Information about daily total solar radiation for each sampling date was obtained from the National Oceanic and Atmospheric Administration (NOAA)

database. From these data, daily PAR surface radiation was computed assuming a factor of 0.48 for the contribution of PAR to total radiation (McCree 1972).

Modifying the expression proposed by Vallina and Simó (2007) for computing solar radiation dose, we calculated a proxy for light availability in the photic layer (LA), considering the magnitude of the surface radiation, the light attenuation coefficient, and the vertical displacements due to turbulent diffusivity as:

$$LA = \frac{I_0}{k * < LO >_{pl}} (1 - exp^{-k * <LO>_{pl}})$$

where I_0, k, and $< LO >_{pl}$ are, respectively, surface PAR irradiance, light attenuation coefficient and photic layer averaged Ozmidov length scale ($LO = (\varepsilon N^{-3})^{1/2}$), which meassures the characteristic length at which stratification restoring forces roughly balance inertial forces in a turbulent flow (Thorpe 2007), and can be interpreted as the extension of vertical displacements of passive particles or organisms.

2.5 Data collected during the TRYNITROP cruise

In order to verify if the results derived from the FAMOSO cruises would extend to other regions, we used data from the TRYNITROP cruise which sampled the tropical and subtropical Atlantic Ocean in April-May 2008. Microstructure turbulence and picoplankton abundance and cell properties were measured in a total of 26 stations during this cruise. Microstructure turbulence was determined by using the same microstructure profiler described for the FAMOSO cruises. Processing routines for these data and the calculation of nitrate diffusive fluxes were similar to those described for the FAMOSO cruises (see above). A description of the methodology used during the TRYNITROP cruise for the determination of nitrate concentration is provided in

225 Mouriño-Carballido et al. (2011), and for the analysis of flow cytometry samples in

226 Calvo-Díaz et al. (2011).

3. Results

3.1 Hydrographic conditions during the FAMOSO cruises

The data obtained by the CTD sensors included in the MSS profiler allowed us to characterize the hydrographic conditions during the FAMOSO cruises (see Figure 2). During F1 (14-22th March) we sampled the early stages of the late winter-early spring bloom (Estrada et al. 2014), when intense mixing of the water column was observed. The depth of the mixed layer, computed as the depth where sigma-t differs by 0.125 from the 10 m value, extended down to ca. 153 m at this cruise. Averaged temperature and salinity values at this layer were 13.1ºC and 38.6, respectively (Table 2). Data collected during F2 (30th Apr-13th May) corresponded to the late stage of the spring bloom. Due to the seasonal warming observed at the surface, the mixed layer averaged over this cruise was shallower (~28 m) and characterized by averaged temperature and salinity values of 15.1ºC and 38.3, respectively. The mixed layer was deeper (~33 m) at the stations sampled during the first part of this cruise (stations 4-25), compared with those stations sampled during the second part (~17 m, stations 29-43). Finally, during F3 (17-19th Sep) we sampled late summer stratification conditions. The mixed layer, which extended down to a depth of ~33 m, was significantly warmer (~23.6ºC) and fresher (~38.2) compared to F1. Relatively increased surface salinity observed during F1 was due to convection of surface waters, cool and salty as a result of evaporation associated to the cold and dry Mistral and Tramontana winds (Leaman & Schott 1991), which mix with deeper salty waters from the Levantine Intermediate Water mass.

The vertical distribution of Brunt-Väisälä frequency (N^2) indicated a progressive increase of the surface stratification from F1 to F3. Averaged N^2 values computed for the nutricline were about 1.7×10^{-5} s^{-2} in F1, 7×10^{-5} s^{-2} in F2 and 16×10^{-5} s^{-2} in F3 (Table 2). As a consequence of local meteorological forcing, in the form of wind stress and

252 buoyancy fluxes (Moum et al. 2001), the vertical distribution of dissipation rates of
253 turbulent kinetic energy (ε) exhibited higher values close to the surface (see also Figure
254 3). Parallel to the progressive warming and stratification of the surface layers, averaged
255 values of ε for the nutricline decreased from F1 (~155x10^{-8} m^2 s^{-3}) to F2 and F3 (~
256 1.2x10^{-8} and 0.4x10^{-8} m^2 s^{-3}, respectively). Because vertical diffusivity (*Kz*) is
257 determined by ε and N^2 distributions (see methods), lower values of *Kz* were observed
258 where vertical stratification was maximum. Averaged *Kz* values for the nutricline were
259 higher at F1 (~70.7x10^{-4} m^2 s^{-1}) compared to F2 (~0.56 x10^{-4} m^2 s^{-1}) and F3 (~0.087x10^{-4} m^2 s^{-1}) (Table 2).
261 Chlorophyll-*a* concentration was higher during F1, when maximum values were located
262 at the surface (1.7±0.5 mg m^{-3}) (Table 2). In comparison to F1, maximum values of
263 chlorophyll during F2 (0.5±0.3 mg m^{-3}) and F3 (0.2±0.1 mg m^{-3}) were lower and
264 located deeper (~50 m in F2 and 60-80 m in F3). Although seasonal changes were clear
265 between cruises, an important variability was observed between stations sampled during
266 each cruise, and between profiles sampled at each station. For example, during F2,
267 stations 19 and 25 were characterized by relatively low values of chlorophyll, whereas
268 higher values were measured at stations 39 and 43. This variability was probably linked
269 to the intense mesoscale and submesoscale activity happening in the region, which was
270 responsible for the important within-cruise variability observed in several physical,
271 chemical and biological properties during this cruise (Estrada et al. 2014).
272 As a result of the progressive increase in stratification and biological uptake (Estrada et
273 al. 2014), surface nitrate concentration decreased from F1 (4.5±1.3 mmolN m^{-3}) to F2
274 (1.7±0.6 mmolN m^{-3}) and F3 (1.3±0.4 mmolN m^{-3}) (Table 2), with similar patterns
275 being observed for phosphate concentration (Figure 3). Despite the observed within-

276 cruise variability, differences in key physical, chemical and biological variables
277 between cruises are clear when observing the averaged profiles (Figure 4).
278
279 *3.2 Picoplankton community composition and cell properties*
280 Higher abundances of picoplankton groups were in general observed at the surface,
281 except for heterotrophic bacteria during F2 (maximum abundance located at ca. 50-80
282 m at station 43), and autotrophic picoplankton during F3, when maxima were
283 sometimes located at 50-80 m, just above the deep chlorophyll maximum (Figure 5).
284 Surface LNA bacteria abundance ranged from $<2x10^5$ cell ml^{-1} during F2 (stations 29,
285 31 and 35) to $>6x10^5$ cell ml^{-1} during F1 (stations 26 and 30). Surface HNA bacteria
286 abundance was also lowest during F2 (stations 25-35, $<2.5x10^5$ cell ml^{-1}) and highest
287 during F1 (stations 26 and 30, $>10x10^5$ cell ml^{-1}). LNA bacteria were in general more
288 abundant than HNA, except during F1. Averaged depth-integrated abundance for these
289 two groups did not differ statistically between cruises, and ranged ca. $1.6\text{-}2.4x10^{13}$ cell
290 m^{-2} (Table 2). *Prochlorococcus* showed low abundance during F1 ($<0.5x10^4$ cell ml^{-1}),
291 was absent during F2, and showed relatively high abundance during F3, when a
292 maximum cell density of ca. $1.9\ x10^5$ cell ml^{-1} was found at 50 m on station 7.
293 Averaged depth-integrated abundance was significantly higher during F3 ($53\pm25\ x10^{11}$
294 cell m^{-2}) compared to F1 ($0.7\pm0.2\ x10^{11}$ cell m^{-2}). Surface *Synechococcus* abundance
295 ranged from 1.6 to $37x10^4$ cell ml^{-1}. The lowest values were found during F3, whereas
296 the highest abundance was sampled during F2 (station 4). Averaged depth-integrated
297 abundance for this group was only statistically higher during F2 ($74\pm50\ x10^{11}$ cell m^{-2})
298 compared to F3 ($9\pm4\ x10^{11}$ cell m^{-2}). Finally, small and large picoeukaryotes abundance
299 exhibited very similar distribution. Their abundance was higher during F1, when peak
300 values of $2.9x10^4$ cell ml^{-1} (small) and $1x10^4$ cell ml^{-1} (large) were measured at the

301 surface at station 23. During F2 and F3, small and large picoeukaryotes abundance was
302 lower than $0.5x10^4$ cell ml^{-1} and $4x10^3$ cell ml^{-1}, respectively. Averaged depth-integrated
303 abundance of small picoeukaryotes was statistically higher during F1 (6 ± 2 $x10^{11}$ cell m^{-2})
304 compared to F2 (1.5 ± 0.5 $x10^{11}$ cell m^{-2}) and F3 (0.5 ± 0.4 $x10^{11}$ cell m^{-2}). For the
305 larger picoeukaryote group the statistical analysis only showed significant differences
306 between F1 (1.9 ± 0.6 $x10^{11}$ cell m^{-2}) and F2 (0.5 ± 0.5 $x10^{11}$ cell m^{-2}).
307 It is remarkable that LNA (0.054 ± 0.003 μm^3) were larger than HNA (0.045 ± 0.003 μm^3)
308 bacteria during F1 (Table 2) (Gomes et al. 2015), whereas the opposite trend, frequently
309 observed in temperate waters (Calvo-Díaz & Morán 2006), was observed during F2 and
310 F3. LNA bacteria were larger during F1 compared to F2, whereas the opposite trend
311 was found for HNA bacteria. *Prochlorococcus* cells were smaller during F1 compared
312 to F3. During F1 *Synechococcus* and small picoeukaryotes were also smaller compared
313 to both F2 and F3. Large picoeukaryotes were smaller during F1 compared to F2.
314 Combining the information of abundance and cell size we determined the contribution
315 of each group to the picoplankton total carbon biomass (Table 2 and Figure 6). Due to
316 the variability observed between the stations sampled at the same cruise, LNA and
317 HNA bacterial biomass did not differ statistically between the three periods.
318 *Prochlorococcus* biomass was higher during F3 (216 ± 12 mg C m^{-2}) compared to F1
319 (3 ± 1 mg C m^{-2}), whereas an increase in *Synechococcus* biomass was observed during F2
320 (871 ± 570 mg C m^{-2}), compared to F1 (325 ± 114 mg C m^{-2}) and F3 (134 ± 57 mg C m^{-2}).
321 Finally small (171 ± 48 mg C m^{-2}) and large (167 ± 52 mg C m^{-2}) picoeukaryotes biomass
322 was higher during F1 compared to F3 (20 ± 14 and 50 ± 21 mg C m^{-2}, respectively).
323 Heterotrophic bacteria were the main contributor to carbon picoplankton biomass except
324 during F2, when the contribution of *Synechococcus* significantly increased up to 51%
325 (Table 2 and Figure 6). *Prochlorococcus* biomass contributed less than 1% during F1

326 and increased up to 21% in F3. Finally, the contribution of small and large
327 picoeukaryotes descreased from F1 (13-14%) to F3 (2-5%).
328
329 *3.3 Correlations between nitrate fluxes and the picoplankton community*
330 The magnitude of nitrate fluxes were the result of the mixing conditions and the vertical
331 nitrate gradient across the nitracline. Mixing conditions, represented by the value of
332 vertical diffusivity, were higher during F1 compared to F2 and F3 (see Table 2 and
333 Figure 2). As a consequence of the increase in stratification, the nitrate gradient across
334 the nitracline increased from F1 (81±49 μmol m^{-4}) to F2 (94±31 μmol m^{-4}) and F3
335 (124±4 μmol m^{-4}), although these differences were not statistically significant as a
336 consequence of the large within-cruise variability. The result of these two patterns was
337 that vertical fluxes of nitrate were higher during F1 (23±35 mmol m^{-2} d^{-1}) compared to
338 F2 (0.4±0.2 mmol m^{-2} d^{-1}) and F3 (0.09±0.09 mmol m^{-2} d^{-1}).
339 No statistically significant relationships were observed between nitrate supply and the
340 depth-integrated abundances of LNA and HNA bacteria, or *Synechococcus,* which was
341 higher at intermediate levels of nitrate supply during F2 (Table 3 and Figure 7).
342 *Prochlorococcus* abundance was negatively correlated with nutrient supply (r^2=-0.726,
343 $p<0.01$), whereas small (r^2=0.686, $p<0.001$) and large (r^2=0.254, $p<0.05$)
344 picoeukaryotes exhibited a positive significant relationship. Nutrient supply showed a
345 positive relationship with the cell size of LNA bacteria, but a negative correlation with
346 that of HNA bacteria, *Prochlorococcus*, *Synechococcus* and small picoeukaryotes
347 (Table 3).
348 In order to summarize our results in the framework of the model proposed by Margalef
349 mandala we plotted the dominance of each picophytoplankton group to total autotrophic
350 picoplankton biomass versus vertical diffusivity, surface nitrate concentration and the

vertical flux of nitrate through turbulent diffusion (Figure 8A). This figure shows that *Prochlorococcus* dominates biomass when nitrate supply was low, *Synechococcus* was dominant at intermediate levels of nitrate supply, and finally the sum of both picoeukaryotic groups dominated biomass under high nutrient supply conditions. As the result of these relationships the ratio of prokaryotic to picoeukaryotic photoautotrophic biomass decreased with nitrate supply (Figure 9B).

Discussion

Control of nutrient supply on picoplankton

Our results clearly show that the model proposed by Margalef can also be applied to the picophytoplankton in the Mediterranean Sea, as the different autotrophic picoplankton types dominated along a gradient in turbulence and nitrate supply in a manner consistent with the larger organisms considered by Margalef (Figure 8A). These results point to different resource requirements of the picophytoplankton groups that are consistent with differential use of new and regenerated forms of nitrogen. *Prochlorococcus* growth has been traditionally considered to be mainly based on regenerated forms of nitrogen (Moore et al. 2002, 2007), though they are also known to assimilate nitrate (Casey et al. 2007, Martiny et al. 2009, Treibergs et al. 2014). *Synechococcus* are able to use a large diversity of new and regenerated forms of nitrogen, including nitrate, nitrite, ammonium, urea, and amino acids (Glibert et al. 1986, Moore et al. 2002, Wawrik et al. 2009). They even can degrade their own phycoerythrin to use as an internal nitrogen source, under extreme nitrogen depleted conditions (Wyman et al. 1985). Eukaryotic phytoplankton can use all forms of fixed nitrogen, and also amino acids and urea (Mulholland & Lomas 2008). A recent study carried out in the Sargasso Sea, combining flow cytometry and isotopic composition, supports the view that prokaryotes rely on recycled nitrogen, whereas small eukaryotes obtains most of its nitrogen demand from upwelled nitrate (Fawcett et al. 2011). Moreover, pigment markers confirms the trophic preferences presented here, as *Prochlorochoccus* are associated with the most oligotrophic conditions, while *Synechococcus* and picoeukaryotes are associated with mesotrophic conditions (Latasa et al. 2010).

Our results showing different responses of picophytoplankton groups to nitrate supply also support the notion that, due to differences in cell size, picophytoplankton groups

have different nutrient uptake capabilities at different nutrient levels. Because smaller cell sizes lead to an increase in nutrient diffusion per unit of cell volume, and a thinning of the diffusion boundary layer around the cell, smaller sizes have a competitive advantage when nutrient availability is low (Chisholm 1992, Kiorboe 1993, Raven 1998). Recent field and laboratory studies indicate that growth rates are similar in both small and large cells but peak at intermediate cell sizes, as the result of trade-off processes related to nutrient requirement, acquisition, and use (Marañón et al. 2014, Marañón 2015). Due to their very small size, *Prochlorococcus* cells are better prepared to cope with extremely low nutrient supply conditions, whereas *Synechococcus* and picoeukaryotes tend to dominate in nitrate-rich waters, due to their faster growth rates at elevated nitrate concentrations. The negative relationship observed between cell size and nutrient supply for *Prochlorococcus*, *Synechococcus* and small picoeukaryotes (see Table 3) could have a physiological explanation. Previous studies have shown that nutrient starvation can limit the division of cells, and that in these conditions an increase in cell size is observed (Latasa & Berdalet 1994). The significant negative relationship reported in our data between cell size and abundance of small picoeukaryotes (Table 3) is in agreement with this mechanism.

The lack of a significant relationship between the abundance of LNA and HNA bacteria and nutrient supply (Figure 7 and Table 3) contradicts the view that bacterial activity is directly controlled by inorganic nutrient inputs (Kirchman 2000). However, the lack of a statistical relationship in our data may have resulted from a relatively narrow range in trophic conditions during our study. Despite not having found any indication of the role of nutrient supply on HNA and LNA bacteria, we cannot discard that potential relationships would have appeared if bacterial growth, instead of bacterial abundance, was used to study the response of bacterial communities.

The use of proxies for estimating nutrient supply

For the first time we used observations of microturbulence in the ocean in order to investigate the influence of mixing and nutrient supply dynamics on picoplankton community structure, in the context of the Margalef´s mandala. Due to the difficulties of measuring turbulence in the field, previous studies have utilized different proxies for nutrient supply, and very often used interchangeably the terms mixing and stratification. Li (2002) showed that as stratification decreases in the North Atlantic there is an increase in large nanoplankton (10-20 μm in diameter), a decrease in picoplankton, and no apparent variation in small nanoplankton, which constitutes the uniform background. Bouman et al (2011) used stratification as a proxy accounting for the three main environmental factors governing phytoplankton growth in the sea: temperature, light and nutrients. By analysing data from the subtropical Pacific, Indian and Atlantic oceans, they observed that picoeukaryotes dominate in well-mixed waters, whereas *Prochlorococcus* are prevalent in strongly stratified regions. Similar patterns were described by Corno et al (2007), who used the lower euphotic zone stratification to describe patterns in the composition of the picoplankton community at the ALOHA time-series station. As far as we know, previous studies focused on the relationship between bacterial abundance and nutrient supply are limited to the study by Gasol et al. (2009), who described a positive relationship between water column stratification and heterotrophic bacterial abundance.

Except for heterotrophic picoplankton, our work is in general consistent with previous studies. However, in the previous studies the relationship between picoplankton abundance and nutrient supply is not obvious as stratification and mixing are not equivalent, neither from a physical perspective nor in their effects on phytoplankton. Vertical diffusivity or mixing refers to the homogenization of gradients of a property. It

can be regarded as the trade-off between the kinetic, and sometimes potential, energy available to drive the turbulence, and the density stratification that can suppress it (Franks 2014). In the field, turbulence is usually measured in terms of the dissipation rate of turbulent kinetic energy, large values indicating that there is a large amount of kinetic energy from turbulence being dissipated at small scales.

During the FAMOSO cruises, and probably in other studies comparing highly contrasting hydrographic regimes, stratification could be a valid proxy for mixing and nutrient supply, as intense stratification conditions are associated with low dissipation rates, low mixing and low nutrient supply (see Table 2). However, increases in turbulence and mixing can also occur in stratified water columns due to, for example, internal waves generation, whose activity and propagation increases with the stratification (Baines 1982). At the shelf edge of the North Sea (Sharples et al. 2007) and the outer part of the Ría de Vigo (Villamaña-Rodríguez et al. 2015), high levels of dissipation rates of turbulent kinetic energy have been described within the stratified pycnocline associated with the breaking internal tide during the spring tides.

The notion that two factors, turbulent mixing and nutrient concentration, determine the magnitude of the nutrient supply was included in the first diagram proposed by Margalef (1978), who chose surface nutrient concentration as the variable representing nutrient availability. From a recent analysis from all major ocean regions Flombaum et al. (2013) concluded that temperature and light are the main factors controlling *Prochlorococcus* and *Synechococcus* distributions, whereas they could not find a clear relationship between nutrient concentration, used in that study as a proxy for nutrient supply, and cell abundance. However, particularly in tropical and subtropical regions the variability in nutrient supply into the surface waters can be disconnected from changes in nutrient concentrations (Mouriño-Carballido et al. 2011). Our results show

457 different responses of picophytoplankton groups to nitrate supply and that, as the result
458 of these relationships, the ratio of prokaryotic to picoeukaryotic photoautotrophic
459 biomass decreased when increasing nitrate supply (Figure 9). However, in this case it is
460 of no consequence if nitrate concentration or nitrate diffusive fluxes are used, as both
461 variables were correlated during the FAMOSO cruises (r^2=0,492; $p<0.001$). In order to
462 investigate if our results would extend to regions where surface nitrate concentration
463 and nitrate diffusive fluxes are clearly disconnected (Mouriño-Carballido et al. 2011),
464 we included data collected in the tropical and subtropical Atlantic during the
465 TRYNITROP cruise (Figure 9). The results from this analysis showed that the observed
466 relationship between nitrate supply and the prokaryotic to picoeukaryotic biomass ratio
467 during the FAMOSO cruises is also valid for the tropical and subtropical Atlantic, but
468 that this relationship only appears when nutrient fluxes, and not surface nutrient
469 concentration, are used as a proxy for nutrient supply.
470
471 *Role of additional factors*
472 Our analysis of the model proposed by Margalef has focussed so far on the role that
473 nutrient supply plays on determining the picoplankton community structure. The model
474 proposed by Margalef is a simplified bottom-up control model including explicitly only
475 two environmental factors (inorganic macro-nutrients and turbulent mixing), placed
476 orthogonally in the diagram although the two axes are not really independent. The use
477 of these two variables accommodates the view that given the scarcity of nutrients and
478 the dissipative effects of turbulent mixing, the pelagic habitat is generally hostile to
479 phytoplankton growth. For this reason the inputs of external energy, on which advection
480 and turbulent mixing depend, control the prominent life forms of phytoplankton.
481 Although not represented in the original diagram, other environmental factors such as

grazing and light availability were discussed by Margalef and are implicitly included in the model. Maximum predator-prey encounter rates occur at an optimum value of turbulent mixing (Lasker 1975), whilst phytoplankton biomass accumulates as grazing pressure lags behind the growth rate of large cells (Kiorboe 1993). The transport of cells through the vertical light gradient also depends on mixing (Vallina & Simó 2007). Light availability was included explicitly in a model proposed by Reynolds (1987), known as the Reynolds's Intaglio, which refines Margalef's axes and predicts the composition of phytoplankton along a gradient of environmental factors (light, nutrients and mixing) (e.g. Smayda and Reynolds 2001). The Intaglio refined the Margalef´s axes, the turbulence axis was replaced by a vector reflecting light availability considering the vertical extent of the mixing, light intensity and its attenuation with depth, whereas the nutrient axis became the accessibility of this resource. The vertical extent of mixing is often represented as the mixed layer depth, typically defined as the shallowest depth at which a difference in temperature or density, measured from the surface, reaches a given threshold (Kara et al. 2000). However, this layer does not necessarily mean a mixing layer, where waters are kept in motion through turbulence (Franks 2014). Modifying the expression proposed by Vallina and Simó (2007) for solar radiation dose, we calculated a proxy for light availability in the photic layer (LA), considering the magnitude of the surface radiation, the light attenuation coefficient, and the vertical displacements due to turbulent diffusivity (see methods). The correlation analysis between LA and picoplankton abundance showed that only large picoeukaryotes (r^2=0.226, $p<0.05$) and *Synechococcus* (r^2=0.357, $p<0.001$), the latter being the only autotrophic picoplankton group which did not correlate significantly with nutrient supply, showed a significant positive relationship with light availability (Table 3).

506 Hence, in our case light availability seems to play a more important role than nutrients
507 in controlling the higher *Synechococcus* abundances sampled during F2 (Figure 8B).
508 We are aware that more data, covering a larger spectrum of hydrographical conditions,
509 will be needed in order to determine the relative contribution of the availability of light
510 and nutrients on structuring the picoplankton community composition. However, the
511 results from this work indicate that nutrient supply was more important than light
512 availability as a control factor responsible for the overall picoplankton composition
513 observed during the FAMOSO cruises in the northwestern Mediterranean Sea (Figure
514 8).
515
516 **Outlook**
517 Autotrophic and heterotrophic picoplankton dominate, numerically as well as in
518 biomass, in oligotrophic highly-stratified regions, such as the subtropical gyres, which
519 could be expanding as a result of global warming (Polovina et al. 2008). It is believed
520 that in these regions, the fate of carbon fixed in the upper layer depends on the
521 composition of picophytoplankton groups (ratio prokaryotes/eukaryotes) (Corno et al.
522 2007). However, our limited understanding about the factors that control picoplankton
523 composition constrains our ability to include them into ocean biogeochemical models,
524 and to predict the consequences of future global change scenarios. For the first time, by
525 using observations in the ocean, we investigated directly the influence of mixing and
526 nutrient supply dynamics on picoplankton community structure in the context of the
527 Margalef´s model. Our results indicate that, in agreement with Margalef's work,
528 picophytoplankton groups exhibit different behaviour to nitrate supply and, as the result
529 of this relationship, the ratio of prokaryotic to picoeukaryotic biomass decreases with
530 increasing nitrate supply. The observed relationship between nitrate supply and the ratio

of prokaryote to picoeukaryote biomass during the FAMOSO cruises is also valid for the tropical and subtropical Atlantic, where surface nitrate concentration and nitrate diffusive fluxes are clearly disconnected. Moreover, in these oligotrophic domains the role of nutrients is only apparent when nitrate diffusive fluxes, and not nutrient concentration, are used. We are aware that our approach ignores other mechanisms potentially important for new nitrogen supply in these regions, such as mesoscale and submesoscale turbulence, lateral transport, atmospheric deposition, nitrogen fixation and more complex three-dimensional dynamics (Jenkins & Doney 2003, Bonnet & Chiaverini 2005, Bonnet et al. 2011, Estrada et al. 2014).

Accurate estimates of nutrient supply are crucial to discern the role that environmental factors play in the composition of picophytoplankton. The utilization of microstructure profilers resolves the old methodological limitations of obtaining accurate estimates of diffusivity, needed to compute the transport of nutrients through the thermocline. They also open a new field of possibilities to get a better understanding of the connection between hydrographic heterogeneities at the marine microscale and diversity, activity, and biogeochemistry of microbial communities (Stocker 2012, Taylor & Stocker 2012).

Acknowledgements

We thank the crew and colleagues on board R. V. Sarmiento de Gamboa and Hespérides for their support during the cruises, and M. Estrada for providing helpful comments about the manuscript. We are very grateful to the detailed comments provided three anonymous reviewers and the editor during the revision process. This work was funded by the Spanish projects TRYNITROP (CTM2004-05174-C02), FAMOSO (CTM2008-06261-C03), TURBIMOC (CTM2009-06712-E/MAR), and CHAOS (CTM2012-30680). P.C. was supported by a Ramon y Cajal fellowship. B. F.-

556 C. thanks the Spanish Government for support through a FPU fellowship (AP2010-
557 5594).

References

Baines PG (1982) On internal tide generation models. Deep Sea Res Part A Oceanogr Res Pap 29:307–338

Bouman HA, Ulloa O, Barlow R, Li WKW, Platt T, Zwirglmaier K, Scanlan DJ, Sathyendranath S (2011) Water-column stratification governs the community structure of subtropical marine picophytoplankton. Environ Microbiol Rep 3:473–482

Bouvier T, Giorgio PA del, Gasol JM (2007) A comparative study of the cytometric characteristics of High and Low nucleic-acid bacterioplankton cells from different aquatic ecosystems. Environ Microbiol 9:2050–2066

Calvo-Díaz A, Ďaz-Pérez L, Suárez LÁ, Morán XAG, Teira E, Marañón E (2011) Decrease in the autotrophic-to-heterotrophic biomass ratio of picoplankton in oligotrophic marine waters due to bottle enclosure. Appl Environ Microbiol 77:5739–5746

Calvo-Díaz A, Morán XAG (2006) Seasonal dynamics of picoplankton in shelf waters of the southern Bay of Biscay. Aquat Microb Ecol 42:159–174

Casey JR, Lomas MW, Mandecki J, Walker DE (2007) Prochlorococcus contributes to new production in the Sargasso Sea deep chlorophyll maximum. Geophys Res Lett 34:1–5

Chisholm S (1992) Phytoplankton Size. In: Falkowski P, Woodhead A (eds) Primary Productivity and Biogeochemical Cycles in the Sea. Plenum Press, New York, p 213–237

Chisholm SW, Olson RJ, Zettler ER, Goericke R, Waterbury JB, Welschmeyer NA (1988) A novel free-living prochlorophyte abundant in the oceanic euphotic zone. Nature 334:340–343

Corno G, Karl DM, Church MJ, Letelier RM, Lukas R, Bidigare RR, Abbott MR (2007) Impact of climate forcing on ecosystem processes in the North Pacific Subtropical Gyre. J Geophys Res 112:C04021

Delgado M, Latasa M, Estrada M (1992) Variability in the size-fractionated distribution of the phytoplankton across the Catalan fron of the north-west Mediterranean. J Plankton Res 14:753–771

Estrada M (1996) Primary production in the northwestern Mediterranean. Sci Mar 60:55–64

Estrada M, Latasa M, Emelianov M, Gutiérrez-Rodríguez A, Fernández-Castro B, Isern-Fontanet J, Mouriño-Carballido B, Salat J, Vidal M (2014) Seasonal and mesoscale variability of primary production in the deep winter-mixing region of the NW Mediterranean. Deep Sea Res Part I Oceanogr Res Pap

595 Fawcett SE, Lomas M, Casey JR, Ward BB, Sigman DM (2011) Assimilation of
596 upwelled nitrate by small eukaryotes in the Sargasso Sea. Nat Geosci 4:717–722

597 Fernández-Castro B, Mouriño-Carballido B, Marañón E, Chouciño P, Gago J, Ramírez
598 T, Vidal M, Bode a., Blasco D, Royer S-J, Estrada M, Simó R (2015) Importance
599 of salt fingering for new nitrogen supply in the oligotrophic ocean. Nat Commun
600 6:8002

601 Flombaum P, Gallegos JL, Gordillo RA, Rincón J, Zabala LL, Jiao N (2013) Present
602 and future global distributions of the marine Cyanobacteria Prochlorococcus and
603 Synechococcus. Proc Natl Acad Sci 110:9824–9829

604 Franks P (2014) Has Sverdrup's critical depth hypothesis been tested? Mixed layers vs.
605 turbulent layers. ICES J Mar Sci J …

606 Gasol JM, Vázquez-Domínguez E, Vaqué D, Agustí S, Duarte CM (2009) Bacterial
607 activity and diffusive nutrient supply in the oligotrophic Central Atlantic Ocean.
608 Aquat Microb Ecol 56:1–12

609 Gasol JM, Zweifel UL, Peters F, Fuhrman JA, Hagstrom A (1999) Significance of size
610 and nucleic acid content heterogeneity as measured by flow cytometry in natural
611 planktonic bacteria. Appl Environ Microbiol 65:4475–4483

612 Glibert PM, Kana TM, Olson RJ, Kirchman DL, Alberte RS (1986) Clonal
613 Comparisons of Growth and Photosynthetic Responses to Nitrogen Availability in
614 Marine Synechococcus Spp. J Exp Mar Bio Ecol 101:199–208

615 Gomes A, Gasol JM, Estrada M, Franco-Vidal L, Díaz-Pérez L, Ferrera I, Morán XAG
616 (2015) Heterotrophic bacterial responses to the winter–spring phytoplankton
617 bloom in open waters of the NW Mediterranean. Deep Sea Res Part I Oceanogr
618 Res Pap 96:59–68

619 Grasshoff K, Kremling K, Ehrhardt M (Eds) (1999) Methods of Seawater Analysis.
620 Wiley-VCH Verlag GmbH, Weinheim

621 Gregg MC, Alford MH, Kontoyiannis H, Zervakis V, Winkel D (2012) Mixing over the
622 steep side of the Cycladic Plateau in the Aegean Sea. J Mar Syst 89:30–47

623 Gutiérrez-Rodríguez A, Latasa M, Estrada M, Vidal M, Marrasé C (2010) Carbon
624 fluxes through major phytoplankton groups during the spring bloom and post-
625 bloom in the Northwestern Mediterranean Sea. Deep Sea Res Part I Oceanogr Res
626 Pap 57:486–500

627 Johnson ZI, Zinser ER, Coe A, McNulty NP, Woodward EMS, Chisholm SW (2006)
628 Niche partitioning among Prochlorococcus ecotypes along ocean-scale
629 environmental gradients. Science 311:1737–1740

630 Kara a. B, Rochford P a., Hurlburt HE (2000) An optimal definition for ocean mixed
631 layer depth. J Geophys Res 105:16803

632 Kiorboe T (1993) Turbulence, phytoplankton cell size, and the structure of pelagic food
633 webs. Adv Mar Biol 29

634 Kirchman DL (2000) Uptake and regeneration of inorganic nutrients by marine
635 heterotrophic bacteria. In: Kirchman DL (ed) Microbial Ecology of the Oceans.
636 John Wiley & Sons, New York, p 261–288

637 Kirk JTO (1994) Light and Photosynthesis in Aquatic Ecosystems. Cambridge
638 University Press

639 Lasker R (1975) Field criteria for survival of anchovy larvae: the relation between
640 inshore chlorophyll maximum layers and successful first feeding. Fish Bull
641 73:453–462

642 Latasa M, Berdalet E (1994) Effect of nitrogen or phosphorus starvation on pigment
643 composition of cultured Heterocaspa sp. J Plankton Res 16:83–94

644 Latasa M, Scharek R, Vidal M, Vila-Reixach G, Gutiérrez-Rodríguez a, Emelianov M,
645 Gasol J (2010) Preferences of phytoplankton groups for waters of different trophic
646 status in the northwestern Mediterranean Sea. Mar Ecol Prog Ser 407:27–42

647 Leaman KD, Schott F (1991) Hydrography structure of the convection regime in the
648 Gulf of Lions: Winter 1987. J Phys Oceanogr 21:575–598

649 Ledwell JR, Ledwell JR, Montgomery ET, Montgomery ET, Polzin KL, Polzin KL, St
650 Laurent LC, St Laurent LC, Schmitt RW, Schmitt RW, Toole JM, Toole JM
651 (2000) Evidence for enhanced mixing over rough topography in the abyssal ocean.
652 Nature 403:179–182

653 Li WKW (2002) Macroecological patterns of phytoplankton in the northwestern North
654 Atlantic Ocean. Nature 419:154–157

655 Li WKW (2007) Macroscopic patterns in marine plankton. In: Levin SA (ed)
656 Encyclopedia of Biodiversity. Elservier1-167, p 1–16

657 Litchman E (2007) Resource competition and ecological success of phytoplankton. In:
658 Falkowski PG, Knoll AH (eds) Evolution of Primary Producers in the Sea.
659 Elservier

660 Longnecker K, Sherr BF, Sherr EB (2005) Activity and phylogenetic diversity of
661 bacterial cells with high and low nucleic acid content and electron transport system
662 activity in an upwelling ecosystem. Appl Environ Microbiol 71:7737–7749

663 MacArthur R, Wilson E. (1967) The theory of island Biogeography (E. Wilson, Ed.).
664 Prince, Princeton

665 Marãnón E, Cermeño P, Huete-Ortega M, López-Sandoval DC, Mouriño-Carballido B,
666 Rodríguez-Ramos T (2014) Resource supply overrides temperature as a controlling
667 factor of marine phytoplankton growth. PLoS One 9:20–23

668 Marañón E (2015) Cell Size as a Key Determinant of Phytoplankton Metabolism and
669 Community Structure. Ann Rev Mar Sci:1–24

670 Margalef R (1978) Life-forms of phytoplankton as survival alternatives in an unstable
671 environment. Oceanol Acta 1:493–509

672 Margalef R, Estrada M, Blasco D (1979) Functional morphology of organims involved
673 in red tides, as adpted to decaying turbulence. In: Taylor DL, Seliger HH (eds)
674 Toxic Dinoflagellates Blooms. Elservier-North Holland, Amsterdam, p 89–94

675 Marie D, Partensky F, Vaulot D (1999) Enumeration of phytoplankton, bacteria, and
676 viruses in marine samples. In: Robinson J (ed) Current protocols in cytometry.
677 John Wiley & Sons, New York, p 11.11.1–11.11.15

678 Martiny AC, Kathuria S, Berube PM (2009) Widespread metabolic potential for nitrite
679 and nitrate assimilation among Prochlorococcus ecotypes. Proc Natl Acad Sci U S
680 A 106:10787–10792

681 McCree KT (1972) The action spectrum, absorptance and quantum yield of
682 photosynthesis in crop plants. Agric For Meteorol 9:191–216

683 Mella-Flores D, Mazard S, Humily F, Partensky F, Mahé F, Bariat L, Courties C, Marie
684 D, Ras J, Mauriac R, Jeanthon C, Mahdi Bendif E, Ostrowski M, Scanlan DJ,
685 Garczarek L (2011) Is the distribution of *Prochlorococcus* and *Synechococcus*
686 ecotypes in the Mediterranean Sea affected by global warming? Biogeosciences
687 8:2785–2804

688 Moore LR, Coe A, Zinser ER, Saito MA, Sullivan MB, Lindell D, Frois-Moniz K,
689 Waterbury J, Chisholm SW (2007) Culturing the marine cyanobacterium
690 Prochlorococcus. Limnol Oceanogr 5:353–362

691 Moore JK, Doney SC, Glover DM, Fung IY (2002) Iron cycling and nutrient-limitation
692 patterns in surface waters of the World Ocean. Deep Res Part II-Topical Stud
693 Oceanogr 49:463–507

694 Morán XAG, Ducklow HW, Erickson M (2011) Single-cell physiological structure and
695 growth rates of heterotrophic bacteria in a temperate estuary (Waquoit Bay,
696 Massachusetts). Limnol Oceanogr 56:37–48

697 Morán XAG, Estrada M (2005) Winter pelagic photosynthesis in the NW
698 Mediterranean. Deep Res Part I-Oceanographic Res Pap 52:1806–1822

699 Mouriño-Carballido B, Graña R, Fernández A, Bode A, Varela M, Domínguez JF,
700 Escánez J, Armas D de, Marañón E (2011) Importance of N-2 fixation vs. nitrate
701 eddy diffusion along a latitudinal transect in the Atlantic Ocean. Limnol Oceanogr
702 56:999–1007

703 Moutin T, Thingstad TF, Wambeke F Van, Marie D, Slawyk G, Raimbault P, Claustre
704 H (2002) Does competition for nanomolar phosphate supply explain the

705 predominance of the cyanobacterium Synechococcus? Limnol Oceanogr 47:1562–
706 1567

707 Mulholland MR, Lomas MW (2008) Nitrogen Uptake and Assimilation. In: Capone
708 DG, Bronk DA, Carpenter DA, Mulholland MR, Carpenter EJ (eds) Nitrogen in
709 the Marine Enviroments. Elservier, p 303–384

710 Norland S (1993) The relationship between biomass and volume of bacteria. In: Kemp
711 P, Sherr B, Sherr E, Cole J (eds) Handboook of Methods in Aquatic Microbial
712 Biology. Lewis Publishers, Boca Raton, FL, p 303–307

713 Oakey NS, Greenan BJW (2004) Mixing in a coastal environment: 2. A view from
714 microstructure measurements. J Geophys Res C Ocean 109:1–17

715 Osborn TR (1980) Estimates of the local rate of vertical diffusion from dissipation
716 meassurements. J Phys Oceanogr 10:83–89

717 Partensky F, Blanchot J, Vaulot D (1999) Differential distribution and ecology of
718 Prochlorococcus and Synechococcus in oceanic waters: a review. Bull l´Institut
719 océanographique 19:457–475

720 Partensky F, Hess WR, Vaulot D (1999) Prochlorococcus, a marine photosynthetic
721 prokaryote of global significance. Microbiol Mol Biol Rev 63:106–127

722 Pianka ER (1970) On r- and K-Selection. Am Nat 104:592–597

723 Polovina JJ, Howell E a., Abecassis M (2008) Oceans least productive waters are
724 expanding. Geophys Res Lett 35:doi: 10.1029/2007GL031745

725 Prandke H, Stips A (1998) Test measurements with an operational microstructure-
726 turbulence profiler: Detection limit of dissipation rates. Aquat Sci 60:191–209

727 Raven JA (1998) The twelfth Tansley Lecture . Small is beautiful : the
728 picophytoplankton. :503–513

729 Reynolds C.S. (1987) Community organization in the freshwater plankton. In: Gee JHR,
730 Giller PS (eds) Organization of Communities, Past and Present. Blackwell, Oxford,
731 p 297–325

732 Richardson TL, Jackson G a (2007) Small phytoplankton and carbon export from the
733 surface ocean. Science 315:838–40

734 Rocap G, Larimer FW, Lamerdin J, Malfatti S, Chain P, Ahlgren NA, Arellano A,
735 Coleman M, Hauser L, Hess WR, Johnson ZI, Land M, Lindell D, Post AF, Regala
736 W, Shah M, Shaw SL, Steglich C, Sullivan MB, Ting CS, Tolonen A, Webb EA,
737 Zinser ER, Chisholm SW (2003) Genome divergence in two Prochlorococcus
738 ecotypes reflects oceanic niche differentiation. Nature 424:1042–1047

739 Scharek R, Latasa M (2007) Growth , grazing and carbon flux of high and low nucleic
740 acid bacteria differ in surface and deep chlorophyll maximum layers in the NW

741 Mediterranean Sea. Aquat Microb Ecol 46:153–161

742 Schattenhofer M, Fuchs BM, Amann R, Zubkov M V, Tarran GA, Pernthaler J (2009)
743 Latitudinal distribution of prokaryotic picoplankton populations in the Atlantic
744 Ocean. Environ Microbiol 11:2078–2093

745 Sharples J, Moore CM, Hickman AE, Holligan PM, Tweddle JF, Palmer MR, Simpson
746 JH (2009) Internal tidal mixing as a control on continental margin ecosystems.
747 Geophys Res Lett 36

748 Sharples J, Moore CM, Rippeth TP, Holligan PM, Hydes DJ, Fisher NR, Simpson JH
749 (2001) Phytoplankton distribution and survival in the thermocline. Limnol
750 Oceanogr 46:486–496

751 Sharples J, Tweddle JF, Green JAM, Palmer MR, Kim Y-N, Hickman AE, Holligan
752 PM, Moore CM, Rippeth TP, Simpson JH, Krivtsov V (2007) Spring-neap
753 modulation of internal tide mixing and vertical nitrate fluxes at a shelf edge in
754 summer. Limnol Oceanogr 52:1735–1747

755 Smayda TJ, Reynolds CS (2001) Community assembly in marine phytoplankton:
756 application of recent models to harmful dinoflagellate blooms. J Plankton Res
757 23:447–461

758 Stocker R (2012) Marine Microbes See a Sea of Gradients. Science 338:628–633

759 Tarran GA, Heywood JL, Zubkov M V (2006) Latitudinal changes in the standing
760 stocks of nano- and picoeukaryotic phytoplankton in the Atlantic Ocean. Deep Res
761 Part II-Topical Stud Oceanogr 53:1516–1529

762 Taylor JR, Stocker R (2012) Trade-Offs of Chemotactic Foraging in Turbulent Water.
763 Science 338:675–679

764 Ternon E, Guieu C, Ridame C, L'Helguen S, Catala P (2011) Longitudinal variability of
765 the biogeochemical role of Mediterranean aerosols in the Mediterranean Sea.
766 Biogeosciences 8:1067–1080

767 Thorpe SA (2007) An introduction to ocean turbulence. Cambrige

768 Treibergs L a., Fawcett SE, Lomas MW, Sigman DM (2014) Nitrogen isotopic response
769 of prokaryotic and eukaryotic phytoplankton to nitrate availability in Sargasso Sea
770 surface waters. Limnol Oceanogr 59:972–985

771 Vallina SM, Simó R (2007) Strong relationship between DMS and the solar radiation
772 dose over the global surface ocean. Science 315:506–508

773 Villamaña-Rodríguez M, Mouriño-Carballido B, Cermeño P, Choucino P, Silva JCB da,
774 Fernández-Castro B, Gilcoto M, Graña R, Latasa M, Marañón E, Otero-Ferrer JL,
775 Scharek R (2015) Role of internal waves on mixing, nutrient supply and
776 phytoplankton composition during spring and neap tides in the Ría de Vigo (NW

777 Iberian Peninsula). In: Aquatic Science Meeting, Granada (Spain).

778 Wawrik B, Callaghan A V, Bronk DA (2009) Use of Inorganic and Organic Nitrogen
779 by Synechococcus spp. and Diatoms on the West Florida Shelf as Measured Using
780 Stable Isotope Probing. Appl Environ Microbiol 75:6662–6670

781 Worden AZ, Nolan JK, Palenik B (2004) Assessing the dynamics and ecology of
782 marine picophytoplankton: The importance of the eukaryotic component. Limnol
783 Oceanogr 49:168–179

784 Wyatt T (2014) Margalef's mandala and phytoplankton bloom strategies. Deep Sea Res
785 Part II Top Stud Oceanogr 101:32–49

786 Wyman M, Gregory RPF, Carr NG (1985) Novel Role for Phycoerythrin in a Marine
787 Cyanobacterium, Synechococcus Strain DC2. Science 230:818–820

788

Table 1. Details of the sampling stations where measurements of microstructure turbulence and cytometry samples were collected during the 2009 FAMOSO cruises (F1, 14-22th March; F2, 30th April – 13th May; and F3, 17-19th September). n indicates the number of microturbulence profiles deployed at each station. Depth refers to the maximum depth reached by the microturbulence profiler.

Cruise	Station	Date	Time (GMT)	Latitude (ºN)	Longitude (°E)	n	Depth (m)
F1	12	14/03/2009	06:34:00	41.583	5.095	7	299
F1	16	15/03/2009	12:56:00	41.500	3.858	7	257
F1	20	18/03/2009	04:58:00	41.459	4.110	7	299
F1	23	19/03/2009	05:00:00	41.618	4.176	7	246
F1	26	21/03/2009	06:11:00	41.819	4.348	7	287
F1	30	22/03/2009	05:45:00	41.793	4.500	7	219
F2	04	30/04/2009	06:00:24	41.500	4.874	7	277
F2	10	03/05/2009	04:56:44	41.496	3.938	6	276
F2	14	04/05/2009	04:36:33	41.547	3.955	7	274
F2	19	07/05/2009	04:59:04	42.106	4.475	7	274
F2	25	08/05/2009	04:52:48	42.023	4.027	7	277
F2	29	09/05/2009	06:56:49	42.040	4.078	7	276
F2	31	10/05/2009	05:35:17	42.057	4.155	7	277
F2	35	11/05/2009	05:29:39	41.471	4.563	7	278
F2	39	12/05/2009	05:34:41	41.401	4.542	7	276
F2	43	13/05/2009	05:33:36	41.352	4.507	7	274
F3	07	17/09/2009	04:20:17	41.472	4.278	7	299
F3	11	18/09/2009	04:23:16	41.463	4.219	7	334
F3	14	19/09/2009	04:18:18	41.928	4.032	7	349

Table 2. Mean values for selected variables collected during the FAMOSO cruises. ε is dissipation rate of turbulent kinetic energy, N^2 Brunt-Väisälä frequency, 1%PAR depth of the 1% of the surface photosynthetically active radiation and LA light availability in the photic layer. Surface values correspond to data collected at ca. 5 m. Nitrate concentrations (abundance and biomass of picoplankton groups) correspond to depth-integrated values for the upper 100 m (down to the photic layer depth). ε, N^2, Vertical diffusivity, nitrate gradients, and diffusive fluxes were calculated across the nutricline (see methods). Cell volume is the averaged volume computed for the photic layer. LNA is low nucleic acid content bacteria, HNA high nucleic acid content bacteria, Proch *Prochlorococcus*, Syne *Synechococcus,* S_picoEuk small picoeukaryotes and L_picoEuk large picoeukaryotes. Contribution (%) of individual groups to total picoplankton biomass is indicated. A nonparametric one-way analysis of variance (Kruskall-Wallis) was performed to test the null hypothesis that independent different groups come from distributions with equal medians. STD is standard deviation calculated using all the profiles deployed at each cruise, and p is statistical probability. The Bonferroni multiple comparison test was applied a posteriori to analyse the differences between every pair of groups (1=F1, 2=F2 and 3=F3). Statistical significance at level α=0.05 (*), α=0.01(**) and α=0.001(***) is indicated.

Variable	F1 (Mean±STD)	F2 (Mean±STD)	F3 (Mean±STD)	Kruskall–Wallis p	Bonferroni comparisons
Surface Temperature (ºC)	13.12±0.03	15.1±0.7	23.6±0.7	<0.001***	1<2,3
Surface Salinity	38.59±0.02	38.30±0.06	38.24±0.03	0.002**	1>2,3
Mixed layer depth (m)	153±105	28±14	33±4	<0.001***	1<2,3
N^2 (s^{-2}) x10^{-5}	1.7±2.7	7.0±8.6	16.0±1.9	<0.001***	1<2<3
ε (m^2 s^{-3}) x10^{-8}	155±4345	1.2±4.6	0.4±1.7	<0.001***	1>2>3
Vertical diffusivity (m^2 s^{-1}) x10^{-4}	70.7±241.9	0.56±0.94	0.087±0.098	<0.001***	1>2>3
Nitrate (0-100 m) (mmol m^{-2})	207±41	186±23	161±21	0.057	
Surface nitrate (mmol m^{-3})	4.5±1.3	1.7±0.6	1.3±0.4	0.002**	1>2,3
Nitrate gradient (µmol m^{-4})	81±49	94±31	124±4	0.144	
Nitrate flux (mmol m^{-2} d^{-1})	23±35	0.4±0.2	0.09±0.09	<0.001***	1>2,3
1% PAR depth (m)	47±5	67±7	75±12	0.004**	1<2,3
Surface PAR (µmol photons m^{-2} s^{-1})	493±42	625±92	411±72	0.004**	2>3
LA (µmol photons m^{-2} s^{-1})	372±115	613±87	379±77	0.004**	1<2>3
Surface chlorophyll a (mg m^{-3})	1.7±0.5	0.5±0.3	0.2±0.1	<0.001***	1>2>3
LNA abundance (cell m^{-2}) x10^{13}	1.64±0.58	2.39±1.33	2.42±0.55	0.216	
HNA abundance (cell m^{-2}) x10^{13}	2.39±1.31	1.66±0.80	2.07±0.71	0.420	
Proch abundance (cell m^{-2}) x10^{11}	0.72±0.23		52.87±24.85	0.020*	1<3
Syne abundance (cell m^{-2}) x10^{11}	26.01±10.56	74.15±50.18	9.10±3.52	0.004**	2>3
S_picoEuk abundance (cell m^{-2}) x10^{11}	5.67±1.82	1.54±0.51	0.49±0.40	<0.001***	1>2,3
L _picoEuK abundance (cell m^{-2}) x10^{11}	1.90±0.60	0.48±0.49	0.66±0.41	0.008**	1>2
LNA cell volume (µm^3 $cell^{-1}$)	0.054±0.003	0.046±0.005	0.046±0.003	0.017*	1>2
HNA cell volume (µm^3 $cell^{-1}$)	0.045±0.003	0.059±0.011	0.059±0.013	0.003**	1<2,3
Proch cell volume (µm^3 $cell^{-1}$)	0.16±0.02		0.3±0.2	0.020*	1<3
Syne cell volume (µm^3 $cell^{-1}$)	0.52±0.04	0.58±0.11	0.67±0.10	0.006**	1<3
S_picoEuk cell volume (µm^3 $cell^{-1}$)	1.30±0.16	1.79±0.29	1.78±0.34	0.003**	1<2
L _picoEuK cell volume (µm^3 $cell^{-1}$)	3.6±0.5	4.9±1.6	3.90±0.78	0.011*	1<2
HNA biomass (mg C m^{-2})	302±166	256±146	328±58	0.623	
LNA biomass (mg C m^{-2})	270±156	316±196	276±38	0.826	
Proch biomass (mg C m^{-2})	3±1		216±12	0.020*	1<3
Syne biomass (mg C m^{-2})	325±114	871±570	134±57	0.002**	2>3
S_picoEuk biomass (mg C m^{-2})	171±48	63±18	20±14	<0.001***	1>2,3
L _picoEuK biomass (mg C m^{-2})	167±52	64±75	50±21	0.019*	1>2
HNA biomass (%)	23±7	16±7	32±3	0.011*	2<3
LNA biomass (%)	21±6	20±8	27±3	0.215	
Proch biomass (%)	0.3±0.1		21±3	<0.001***	1<3
Syne biomass (%)	24±4	51±18	11±5	0.004**	2>3
S_picoEuk biomass (%)	14±4	4±4	2±1	<0.001**	1>2,3
L _picoEuK biomass (%)	13±3	4±3	5±2	0.003**	1>2

Table 3. Squared Pearson correlation coefficients (r^2) for photic layer depth-integrated abundance, averaged cell volume in the photic layer, vertical diffusive flux of nitrate and light availability in the photic layer (LA) calculated for the FAMOSO cruises. LNA and HNA refers to low and high nucleic acid content bacteria, respectively, Small picoEuk to small picoeukaryotes and Large picoEuk to large picoeukaryotes. Statistical significance level (*p*) is noted as * $p<0.05$, ** $p<0.01$, and *** $p<0.001$. For simplicity only statistical significant relationships are shown. Variables which did not follow normal distributions were log-transformed.

	Log Biovolume r^2	Log nitrate flux r^2	*LA* r^2
Abundance LNA			
Abundance HNA			
Log Abundance *Prochlorococcus*	0.903 ***	-0.726**	
Log Abundance *Synechococcus*			0.357***
Log Abundance Small picoEuk	-0.584***	0.686***	
Log Abundance Large picoEuk		0.254*	0.226*
Cell volume LNA		0.287*	
Cell volume HNA		-0.507***	
Log cell volume *Prochlorococcus*		-0.799**	
Log cell volume *Synechococcus*		-0.372**	
Log cell volume Small picoEuk		-0.526***	
Log cell volume Large picoEuk			

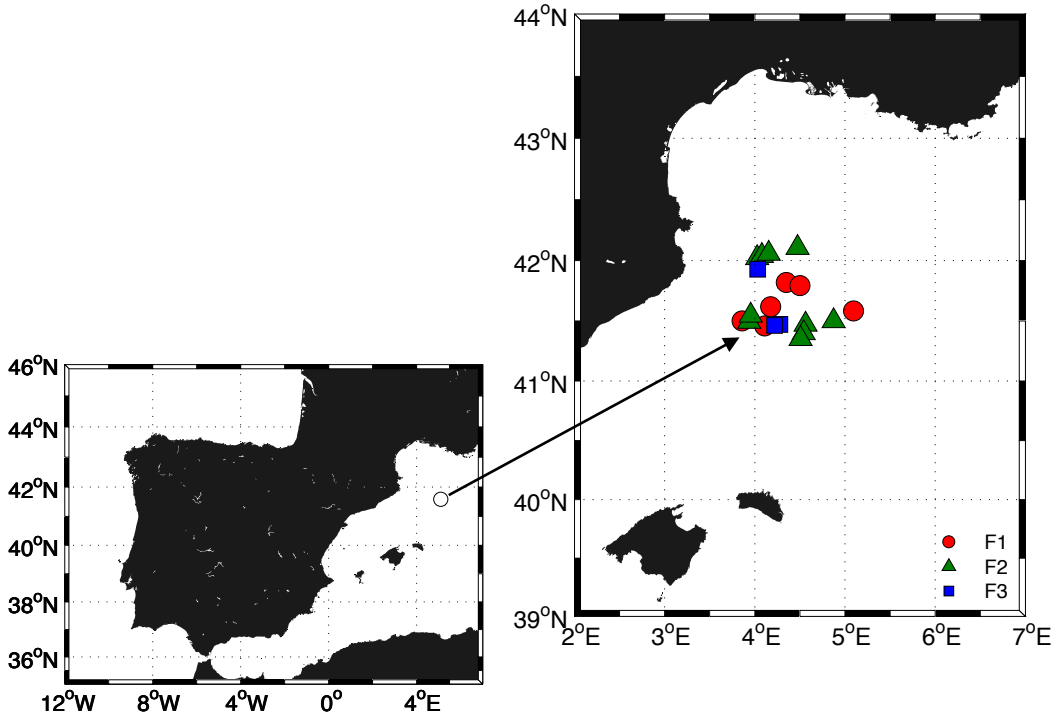

Figure 1. Map of the location where microturbulence profiles were conducted during the 2009 FAMOSO cruises (F1, 14-22th March, circles; F2, 30th April – 13th May, crosses; F3, 17-19th September, squares). Details about the sampling stations are shown in Table 1.

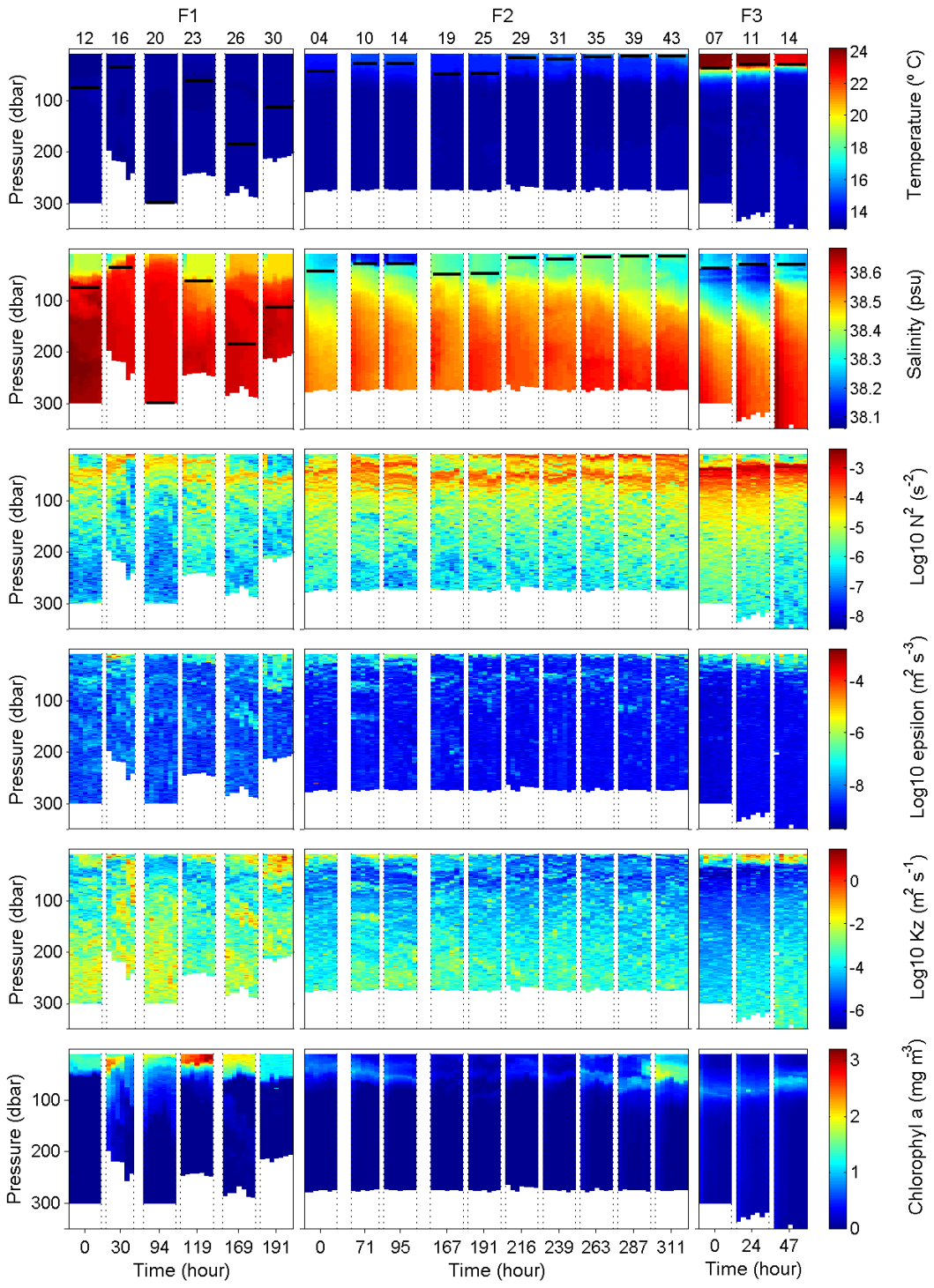

Figure 2. Vertical distribution of temperature (ºC), salinity (psu), Brünt-Väissäla frequency (s^{-2}, note the logarithmic scale), dissipation rates of turbulent kinetic energy (m^2 s^{-3}, note the logarithmic scale), vertical diffusivity (Kz, m^2 s^{-1}, note the logarithmic scale) and chlorophyll-a (mg m^{-3}) measured with the microturbulence profiler during the FAMOSO cruises. The black line represents the averaged mixed layer depth computed for each station as the depth where sigma-t differs 0.125 from the 10 m value. Numbers at the top indicate station numbers (see Table 1). For each station the 6-7 microturbulence profiles deployed are plotted. Time between stations is not proportional to the time scale plotted in the x axis.

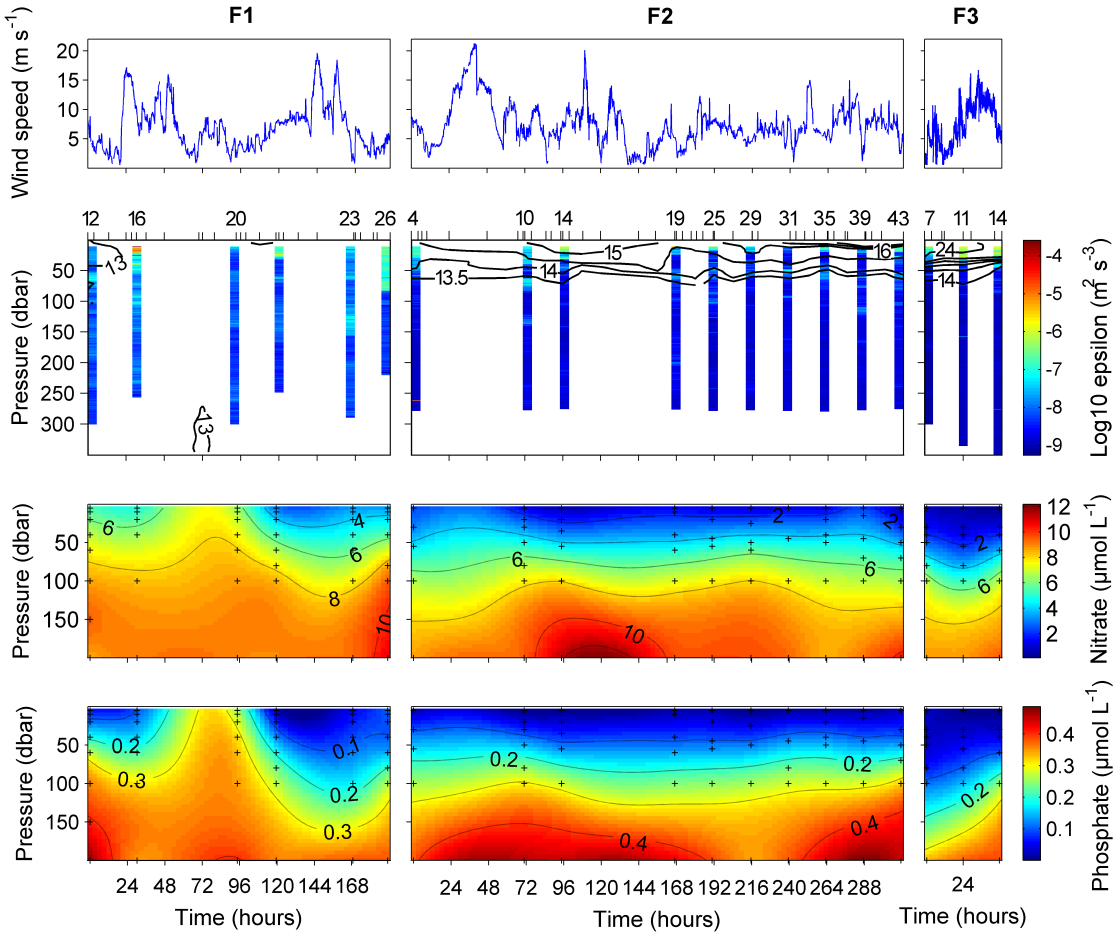

Figure 3. Wind speed and vertical distribution of dissipation rates of turbulent kinetic energy (epsilon, superimposed to isotherms), nitrate and phosphate concentration sampled during the FAMOSO cruises. Numbers at the top correspond to stations (see Table 1) and ticks indicate all the CTD casts deployed at each cruise. Epsilon profiles correspond to averaged values computed from the 6-7 profiles deployed at each station.

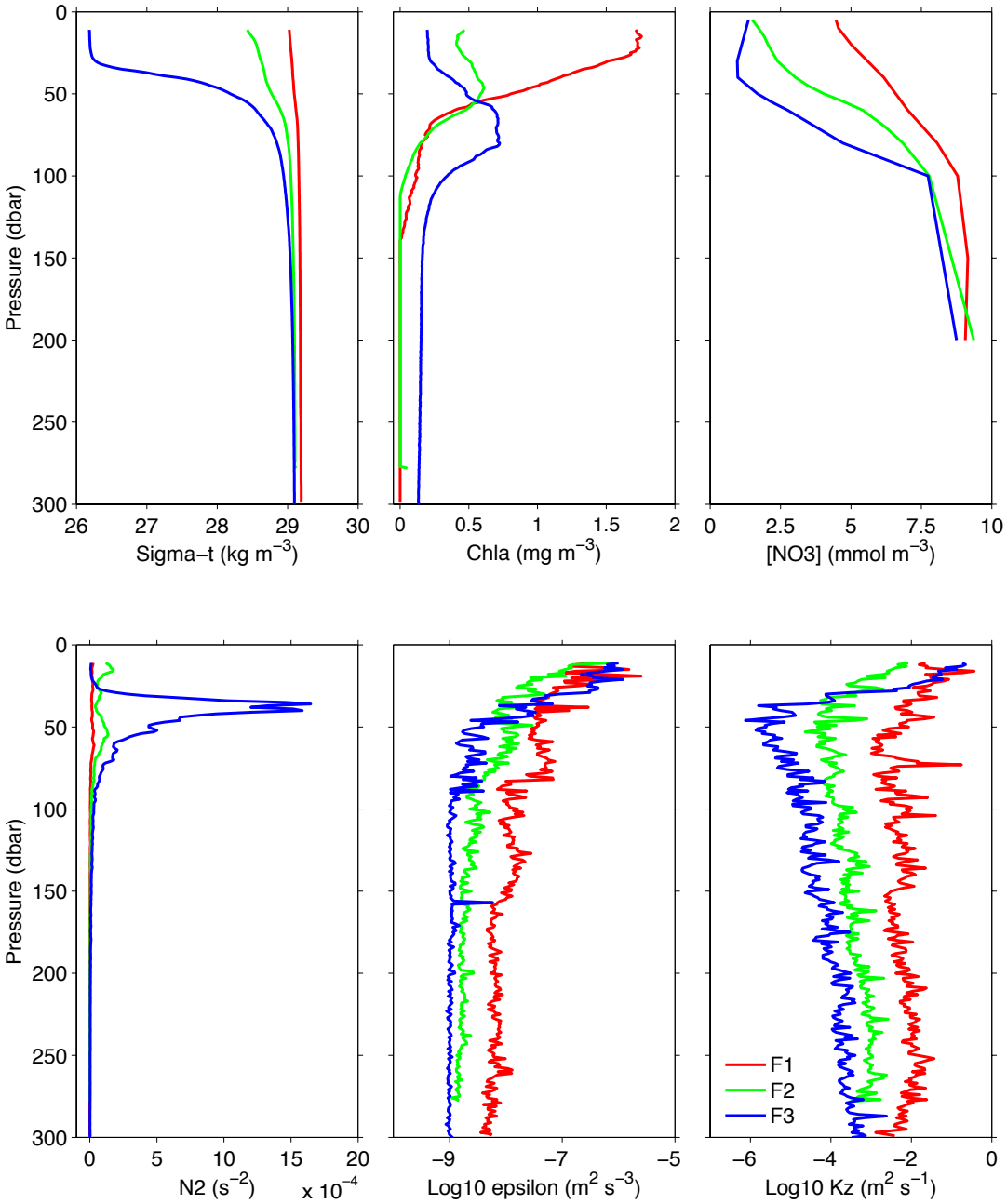

Figure 4. Averaged vertical distribution of sigma-t, chlorophyll-a, nitrate concentration, Brünt Väissäla frequency, dissipation rates of turbulent kinetic energy (epsilon, note the logarithmic scale), and vertical diffusivity (Kz, note the logarithmic scale) measured with the microturbulence profiler during the FAMOSO cruises.

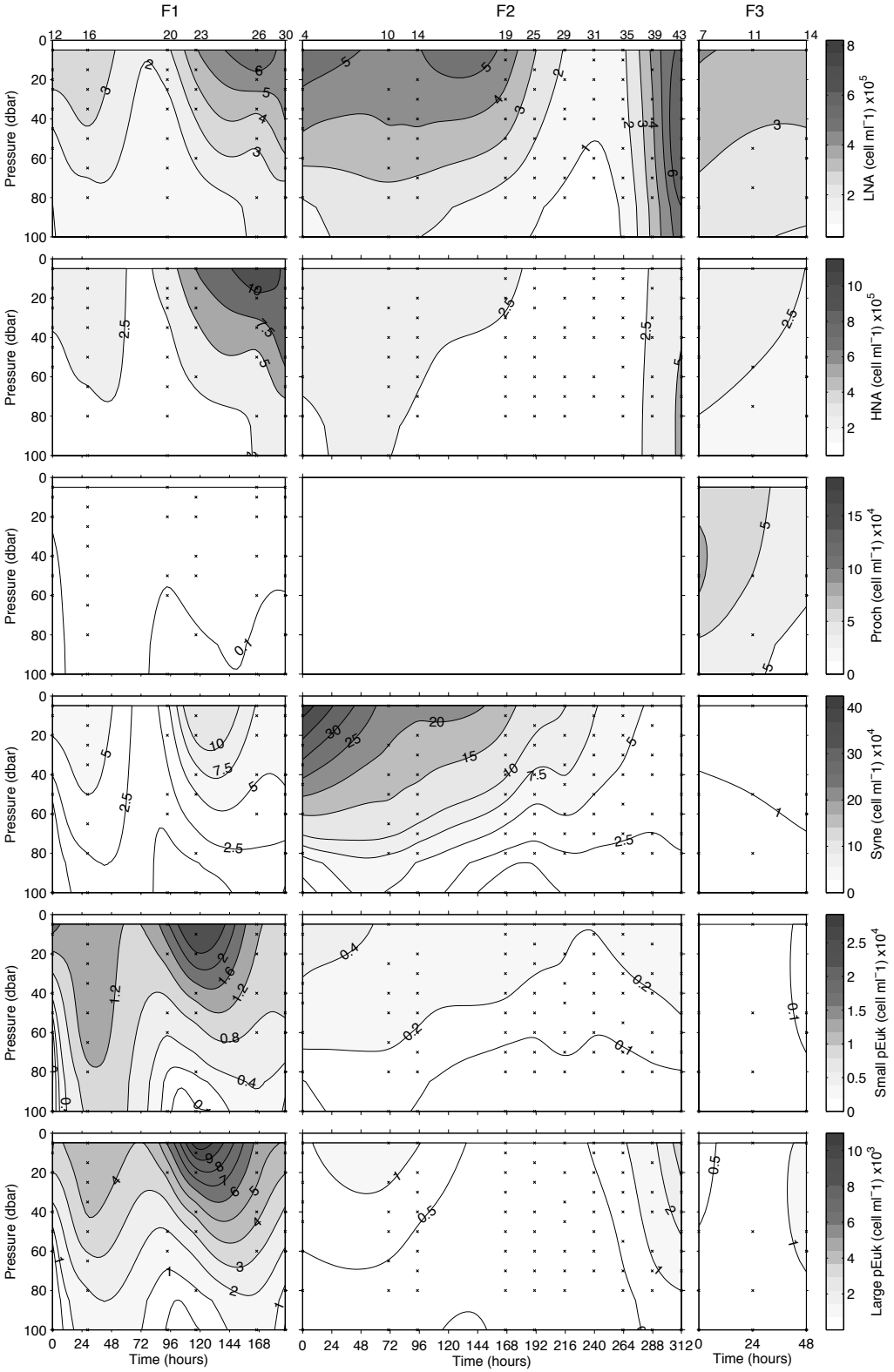

Figure 5. Vertical distribution of abundance of low nucleic acid content bacteria (LNA), high nucleic acid content bacteria (HNA), *Prochlorococcus*, *Synechococcus,* small picoeukaryotes and large picoeukaryotes abundance (cell ml^{-1}) during the FAMOSO cruises. Numbers at the top indicate station numbers (see Table 1).

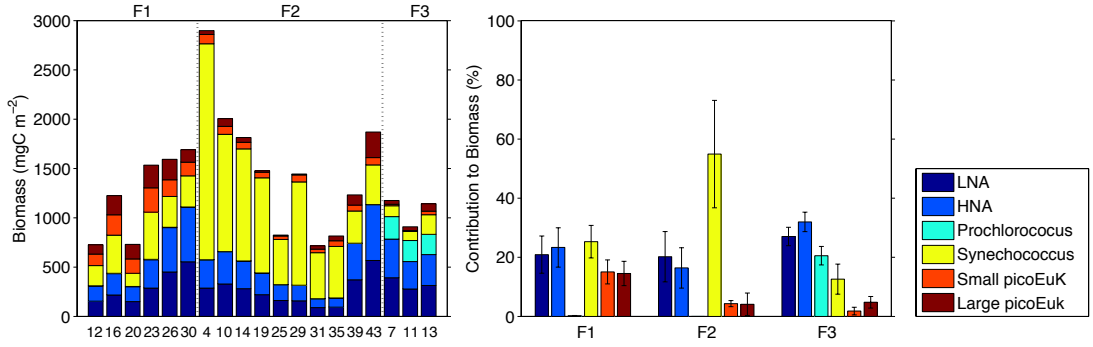

Figure 6. Photic layer depth-integrated biomass (left) and averaged contribution to total picoplankton biomass (right) of LNA and HNA bacteria, *Prochlorococcus*, *Synechococcus*, Small and Large picoeukaryotes during the FAMOSO cruises. Numbers at the bottom indicate station numbers (see Table 1). Erros bars correspond to standard deviation.

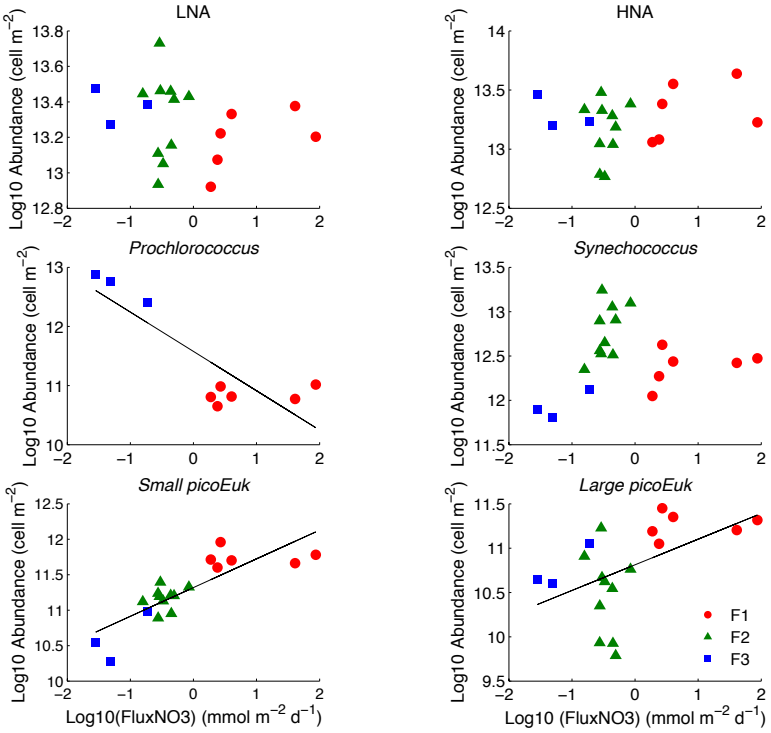

Figure 7. Relationship between abundance of low (LNA) and high (HNA) nucleic acid content bacteria, *Prochlorococcus*, *Synechococcus,* small picoeukaryotes and large picoeukaryotes and vertical diffusive flux of nitrate computed for the FAMOSO cruises. The black lines represent the lineal fit for those relationships which, by using the total data collected during the three cruises, were statistically significant (see Table 3). Variables which did not follow normal distributions were log-transformed.

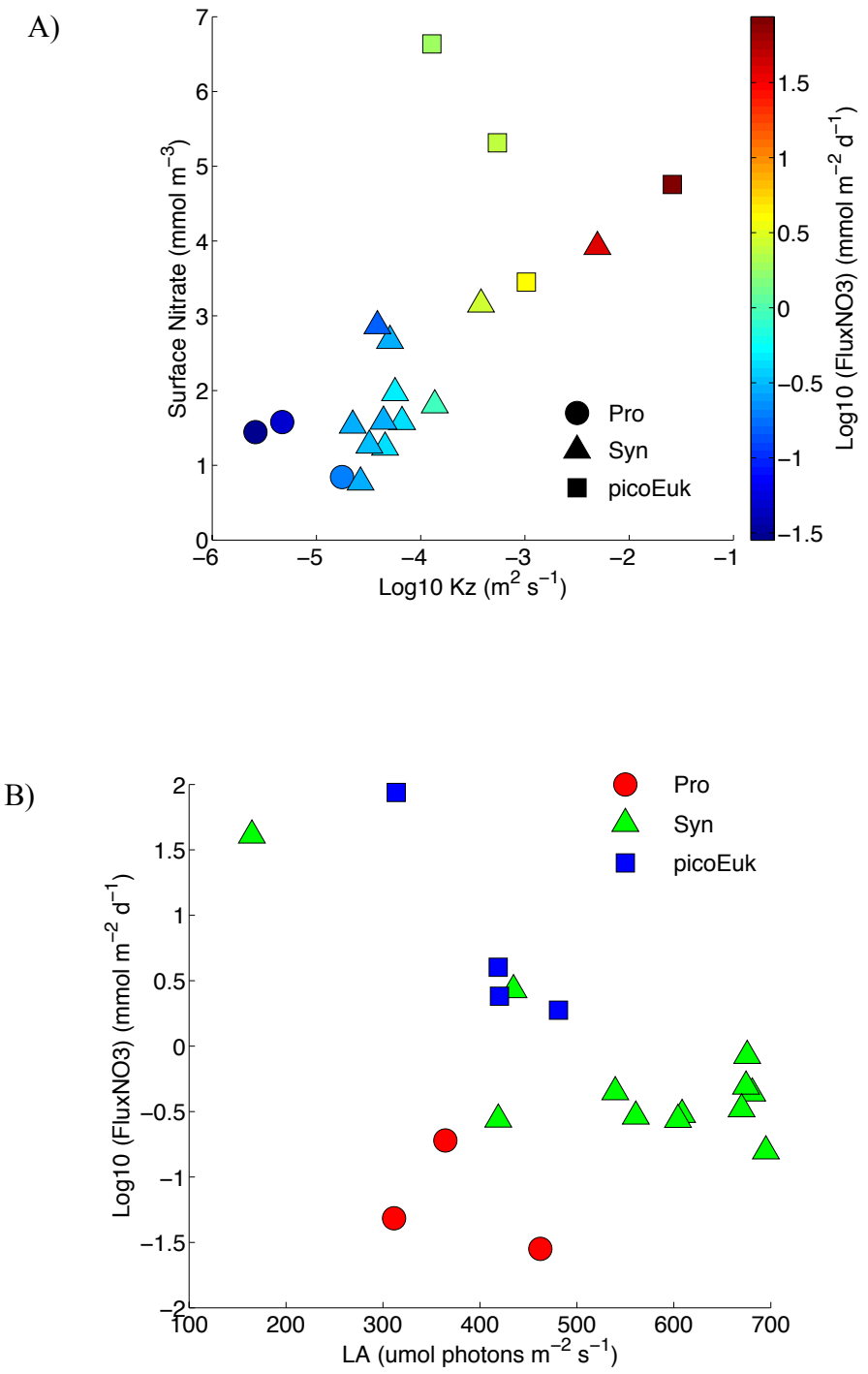

Figure 8. Dominance of *Prochlorococcus* (circles), *Synechococcus* (triangles) or picoeukaryotes (including large and small sizes, squares) versus A) vertical diffusivity, surface nitrate concentration and vertical flux of nitrate through turbulent diffusion (color bar), and B) light availability in the photic layer (LA) and vertical flux of nitrate through turbulent diffusion computed for the FAMOSO cruises. Dominance means that the group represented the major contribution to total autotrophic picoplankton biomass.

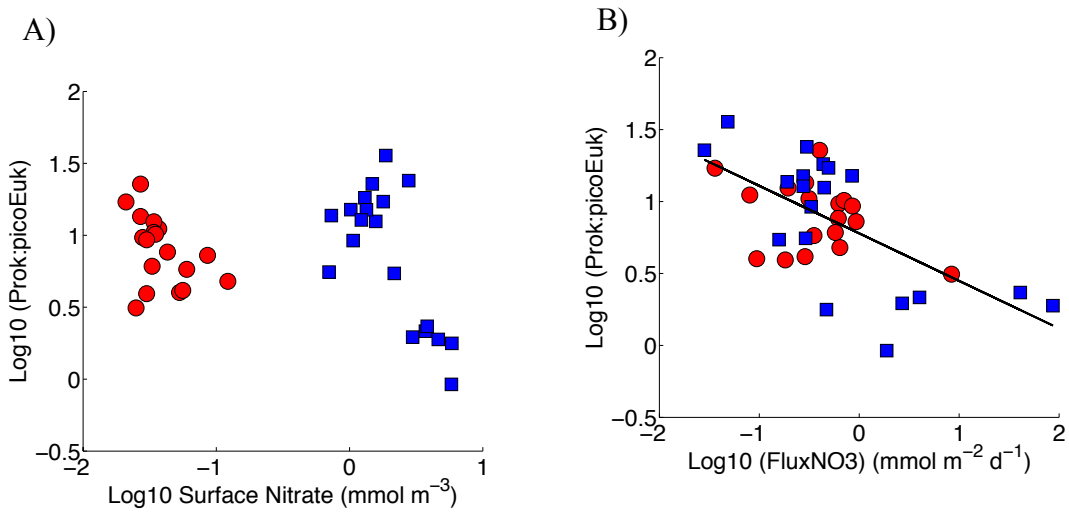

Figure 9. Ratio of prokaryotes to picoeukariotes (only including small picoeukaryotes) photic layer depth-integrated biomass versus (A) nitrate concentration and (B) vertical diffusive flux of nitrate during the FAMOSO (blue squares) and the TRYNITROP cruises (red circles, tropical and subtropical Atlantic). The black line indicates the statistically significant relationship (r^2=0.395; $p<0.001$) calculated using data from both the FAMOSO and the TRYNITROP cruises.